Controlling the effective second-order susceptibility in random quadratic media

Mousa Ayoub,* Markus Paßlick, Jörg Imbrock, and Cornelia Denz

Institute of Applied Physics and Center for Nonlinear Science (CeNoS), University of Münster, Corrensstr. 2, 48149 Münster, Germany

*ayoubm@uni-muenster.de

Abstract: We study systematically the effect of spatial disorder of ferroelectric domains in nonlinear media on the polarization properties of optical frequency conversion. Experimentally, different statistics of domain sizes are created using electric field poling at room temperature. We analyze the evolution of polarization properties of the second- and third-harmonic signals for each created statistic by determining the corresponding relative strength of non-zero components of the second-order susceptibility tensor, d_{24}, d_{32} and d_{33}. The relative strengths are labeled by means of the control parameter E on the characteristic P-E loop of the studied ferroelectric medium.

© 2015 Optical Society of America

OCIS codes: (190.0190) Nonlinear optics; (190.4410) Nonlinear optics, parametric processes; (190.4975) Parametric processes; (160.2260) Ferroelectrics.

References and links

1. J. Trull, C. Cojocaru, R. Fischer, S. M. Saltiel, K. Staliunas, R. Herrero, R. Vilaseca, D. N. Neshev, W. Krolikowski, and Y. S. Kivshar, "Second-harmonic parametric scattering in ferroelectric crystals with disordered nonlinear domain structures," Opt. Express **15**, 15868–15877 (2007).
2. V. Berger, "Nonlinear photonic crystals," Phys. Rev. Lett. **81**, 4136–4139 (1998).
3. A. R. Tunyagi, M. Ulex, and K. Betzler, "Noncollinear optical frequency doubling in strontium barium niobate," Phys. Rev. Lett. **90**, 243901 (2003).
4. R. Fischer, S. M. Saltiel, D. N. Neshev, W. Krolikowski, and Y. S. Kivshar, "Broadband femtosecond frequency doubling in random media," Appl. Phys. Lett. **89**, 191105 (2006).
5. P. Molina, S. Álvarez García, M. O. Ramírez, J. García-Solé, L. E. Bausá, H. Zhang, W. Gao, J. Wang, and M. Jiang, "Nonlinear prism based on the natural ferroelectric domain structure in calcium barium niobate," Appl. Phys. Lett. **94**, 071111 (2009).
6. M. Ayoub, P. Roedig, J. Imbrock, and C. Denz, "Domain-shape-based modulation of Čerenkov second-harmonic generation in multidomain strontium barium niobate," Opt. Lett. **36**, 4371–4373 (2011).
7. K. A. Kuznetsov, G. K. Kitaeva, A. V. Shevlyuga, L. I. Ivleva, and T. R. Volk, "Second harmonic generation in a strontium barium niobate crystal with a random domain structure," JETP Letters **87**, 98–102 (2008).
8. P. Molina, M. de la O Ramírez, and L. E. Bausá, "Strontium barium niobate as a multifunctional two-dimensional nonlinear âĂŸphotonic glassâĂŹ," Adv. Funct. Mater. **18**, 709–715 (2008).
9. Y. Sheng, J. Dou, B. Ma, B. Cheng, and D. Zhang, "Broadband efficient second harmonic generation in media with a short-range order," Appl. Phys. Lett. **91**, 011101 (2007).
10. S. Kawai, T. Ogawa, H. S. Lee, R. C. DeMattei, and R. S. Feigelson, "Second-harmonic generation from needle-like ferroelectric domains in $Sr_{0.6}Ba_{0.4}Nd_2O_6$ single crystals," Appl. Phys. Lett. **73**, 768–770 (1998).
11. M. Ayoub, J. Imbrock, and C. Denz, "Second harmonic generation in multi-domain χ^2 media: from disorder to order," Opt. Express **19**, 11340–11354 (2011).
12. R. Fischer, D. N. Neshev, S. M. Saltiel, A. A. Sukhorukov, W. Krolikowski, and Y. S. Kivshar, "Monitoring ultrashort pulses by transverse frequency doubling of counterpropagating pulses in random media," Appl. Phys. Lett. **91**, 031104 (2007).

#251216 Received 30 Sep 2015; revised 11 Nov 2015; accepted 17 Nov 2015; published 24 Dec 2015
© 2015 OSA

13. J. Trull, S. Saltiel, V. Roppo, C. Cojocaru, D. Dumay, W. Krolikowski, D. Neshev, R. Vilaseca, K. Staliunas, and Y. Kivshar, "Characterization of femtosecond pulses via transverse second-harmonic generation in random nonlinear media," Appl. Phys. B **95**, 609–615 (2009).
14. D. Dumay, S. M. Saltiel, D. N. Neshev, W. Krolikowski, and Y. S. Kivshar, "Pulse measurements by randomly quasi phase matched second harmonic generation in the regime of total internal reflection," J. Phys. B **42**, 175403 (2009).
15. J. Trull, I. Sola, B. Wang, A. Parra, W. Krolikowski, Y. Sheng, R. Vilaseca, and C. Cojocaru, "Ultrashort pulse chirp measurement via transverse second-harmonic generation in strontium barium niobate crystal," Appl. Phys. Lett. **106**, 221108 (2015).
16. D. Viehland, Z. Xu, and W.-H. Huang, "Structure-property relationships in strontium barium niobate I. needle-like nanopolar domains and the metastably-locked incommensurate structure," Philosophical Magazine A **71**, 205–217 (1995).
17. P. Lehnen, W. Kleemann, T. Woike, and R. Pankrath, "Ferroelectric nanodomains in the uniaxial relaxor system $Sr_{0.61-x}Ba_{0.39}Nb_2O_6$:$Ce_x^{3+}$," Phys. Rev. B **64**, 224109 (2001).
18. J. Dec, V. V. Shvartsman, and W. Kleemann, "Domainlike precursor clusters in the paraelectric phase of the uniaxial relaxor $Sr_{0.61}Ba_{0.39}Nb_2O_6$," Appl. Phys. Lett. **89**, 212901 (2006).
19. L. Tian, D. A. Scrymgeour, and V. Gopalan, "Real-time study of domain dynamics in ferroelectric $Sr_{0.61}Ba_{0.39}Nb_2O_6$," J. Appl. Phys. **97**, 114111 (2005).
20. M. Ayoub, M. Paßlick, K. Koynov, J. Imbrock, and C. Denz, "Effect of the domain shape on noncollinear second-harmonic emission in disordered quadratic media," Opt. Express **21**, 31462–31468 (2013).
21. Y. Le Grand, D. Rouede, C. Odin, R. Aubry, and S. Mattauch, "Second-harmonic scattering by ferroelectric domains in rbh_2po_4," Ferroelectrics **273**, 217–222 (2002).
22. K. Terabe, S. Takekawa, M. Nakamura, K. Kitamura, S. Higuchi, Y. Gotoh, and A. Gruverman, "Imaging and engineering the nanoscale-domain structure of a $Sr_{0.61}Ba_{0.39}Nb_2O_6$ crystal using a scanning force microscope," Appl. Phys. Lett. **81**, 2044–2046 (2002).
23. W. Wang, K. Kalinowski, V. Roppo, Y. Sheng, K. Koynov, Y. Kong, C. Cojocaru, J. Trull, R. Vilaseca, and W. Krolikowski, "Second- and third-harmonic parametric scattering in disordered quadratic media," J. Phys. B **43**, 215404 (2010).
24. M. Ayoub, P. Roedig, K. Koynov, J. Imbrock, and C. Denz, "Čerenkov-type second-harmonic spectroscopy in random nonlinear photonic structures," Opt. Express **21**, 8220–8230 (2013).
25. L. Mateos, P. Molina, J. F. Galisteo-Lopez, C. Lopez, L. E. Bausa, and M. O. Ramirez, "Ultrabroadband generation of multiple concurrent nonlinear coherent interactions in random quadratic media," Appl. Phys. Lett. **103**, 101101 (2013).
26. M. Baudrier-Raybaut, R. Haidar, P. Kupecek, P. Lemasson, and E. Rosencher, "Random quasi-phase-matching in bulk polycrystalline isotropic nonlinear materials," Nature **432**, 374–376 (2004).
27. A. S. Aleksandrovsky, A. M. Vyunishev, I. E. Shakhura, A. I. Zaitsev, and A. V. Zamkov, "Random quasi-phase-matching in a nonlinear photonic crystal structure of strontium tetraborate," Phys. Rev. A **78**, 031802 (2008).
28. Y. Le Grand, D. Rouede, C. Odin, R. Aubry, and S. Mattauch, "Second-harmonic scattering by domains in RbH_2PO_4 ferroelectrics," Opt. Commun. **200**, 249–260 (2001).
29. U. Voelker, U. Heine, C. Gödecker, and K. Betzler, "Domain size effects in a uniaxial ferroelectric relaxor system: The case of $Sr_xBa_{1-x}Nb_2O_6$," J. Appl. Phys. **102**, 114112 (2007).
30. Y. Sheng, A. Best, H.-J. Butt, W. Krolikowski, A. Arie, and K. Koynov, "Three-dimensional ferroelectric domain visualization by Čerenkov-type second harmonic generation," Opt. Express **18**, 16539–16545 (2010).
31. K. Megumi, N. Nagatsuma, Y. Kashiwada, and Y. Furuhata, "The congruent melting composition of strontium barium niobate," J. Mater. Sci. **11**, 1583–1592 (1976).
32. M. Horowitz, A. Bekker, and B. Fischer, "Broadband second-harmonic generation in $Sr_xBa_{1x}Nb_2O_6$ by spread spectrum phase matching with controllable domain gratings," Appl. Phys. Lett. **62**, 2619–2621 (1993).
33. C. R. Jeggo and G. D. Boyd, "Nonlinear optical polarizability of the niobiumoxygen bond," J. Appl. Phys. **41**, 2741–2743 (1970).
34. N. Fujioka, S. Ashihara, H. Ono, T. Shimura, and K. Kuroda, "Cascaded third-harmonic generation of ultrashort optical pulses in two-dimensional quasi-phase-matching gratings," J. Opt. Soc. Am. B **24**, 2394–2405 (2007).
35. O. Pfister, J. S. Wells, L. Zink, D. A. V. Baak, M. D. Levenson, and W. R. Bosenberg, "Continuous-wave frequency tripling and quadrupling by simultaneous three-wave mixings in periodically poled crystals: application to a two-step 1.19–10.71-μm frequency bridge," Opt. Lett. **22**, 1211–1213 (1997).
36. W. Wang, V. Roppo, K. Kalinowski, Y. Kong, D. N. Neshev, C. Cojocaru, J. Trull, R. Vilaseca, K. Staliunas, W. Krolikowski, S. M. Saltiel, and Y. Kivshar, "Third-harmonic generation via broadband cascading in disordered quadratic nonlinear media," Opt. Express **17**, 20117–20123 (2009).

#251216 Received 30 Sep 2015; revised 11 Nov 2015; accepted 17 Nov 2015; published 24 Dec 2015
© 2015 OSA

1. Introduction

In general, the analysis of the allowed polarization in nonlinear parametric processes is part and parcel of nonlinear optics. As is well known, the symmetry of the nonlinear medium determines the non-zero components of the nonlinear susceptibility tensor. The relative relation between these components relates in turn to the spatial distribution of the nonlinearity [1]. Quasi-phase matching is an applicable way out of the phase-matching problem, it is however restricted to a fixed input wavelength and a single interaction due to the single period nonlinearity. This concept can be extended to a two-dimensional (2D) modulation of the quadratic nonlinearity [2] called nonlinear photonic crystals (NPCs). It has been shown that nonlinear media with disordered nonlinear polarization structures can be an excellent platform to broaden the bandwidth of the interaction [3–5]. That opens the door to an incoherent superposition of parametric processes [1]. Multi-dimensional disorder provides the possibility to apply different noncollinear phase-matching conditions, classified into two main categories: longitudinal (also named Čerenkov condition [6]), due to which the second-harmonic signal is emitted on a cone [3,4,7,8] and lateral (nonlinear Bragg condition [9]), for which the harmonics are emitted in a plane [4,10,11]. Those broadband noncollinear phase-matching processes can also be used to characterize femtosecond laser pulses [12–15].

Recently, random strontium barium niobate (RSBN) crystals have been adopted as one of the most interesting platforms for the investigation of nonlinear interactions and harmonic generations due to their natural inherent disorder. The randomness is manifested as a random or short-range ordered domain distribution defined by the poling state [8,9,11]. SBN crystals are of 4mm symmetry and possess needle-like domain structures elongated parallel to the crystal's polar axis [16] with a wide variety of length scale at the polar-end faces [17,18]. The domain cross-sections are squares with rounded corners corresponding to the crystal symmetry. They can build very complex fractal-like patterns [19,20]. These patterns posses in turn an irregular spatial distribution due to the random domain size and the spatial position. The sizes are normal distributed as in [21] with a certain mean width a and variance σ. This is reflected in a wide spectrum of $\chi^{(2)}$ reciprocal k vectors, which are necessary to compensate for the phase mismatch of the phase velocities of the fundamental and second-harmonic beams interacting inside the nonlinear volume. The reported domain widths in SBN crystals range between a few nanometers and a few micrometers and the lengths are of a few hundreds of micrometers [22]. Due to this broad spectrum of domain widths, the higher harmonics intensity distribution can look very different [11,23]. Moreover, the effect imposed by the randomness on the SH far-field distribution provides the possibility to deduce the ferroelectric domain statistics inside the medium [20,24].

The aim of this work is to control the contribution of each process allowed by the nonlinearity tensor of SBN by affecting the corresponding coefficients by controlled variation of domain size distribution. With that, we systematically demonstrate the ability to control the interplay of the different processes. We also examine the nature of the interaction between them, which ranges between coherent [25] and incoherent interactions [1]. A simplified concept is depicted in Fig. 1. For nanoscaled domains, the strong Fourier coefficients lie on a broad circle [see Fig. 1(a)] whereas for microscaled domains, the largest coefficients move to the center of the Fourier space [see Fig. 1(b)]. Since the SH intensity is proportional to the square of the coefficients, which satisfy the phase-matching condition, every parametric process clearly depends on the strength of those coefficients. Here, we actively change this strength. Up to now all experiments published by other groups are restricted on a domain size distribution determined by the natural growth of crystals, in which the average domain size strongly differs from one sample to another. For that, the characteristic hysteresis loop of the ferroelectric SBN is recorded. Every change in the domain statistic is represented by the spontaneous polarization, which is

#251216 Received 30 Sep 2015; revised 11 Nov 2015; accepted 17 Nov 2015; published 24 Dec 2015
© 2015 OSA

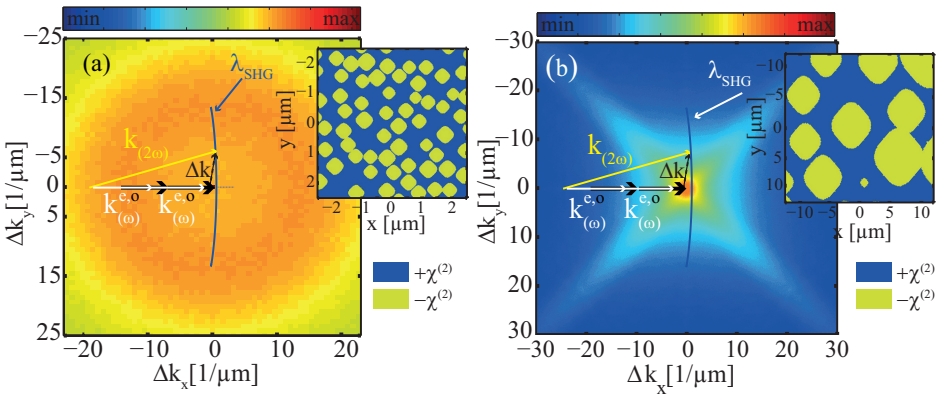

Fig. 1. (a, b) Fourier spectra for the two averaged domain sizes 0.25 µm and 3.5 µm, respectively. Insets: The corresponding modeled real space of random "$+\chi^{(2)}$" and "$-\chi^{(2)}$" structure. The noncollinear Bragg phase-matching condition, which leads to broad SH intensity distribution is schematically illustrated for the ordinarily and extraordinarily polarized input beams.

in turn labeled on the hysteresis curve. Thus, it is not only possible to control the processes, but also to restore the desired interaction strength by adjusting the corresponding spontaneous polarization.

2. Harmonics analyzing setup

A particularly successful way to create different statistics is to excite the domain walls to move or to grow randomly in the volume. Applying an external electric field along the crystallographic axis above the coercive field will switch the domains. The switching process takes place in SBN in an incomplete way. This imperfection is called *aging* effect. Taking advantage of the existence of the aging effect, each switching process leads to different domain size statistics [11], without losing the random nature of the domain structures [20] [see Fig. 2]. This concept has been applied on different random systems like polycrystalline ferroelectrics [26], and crystals with randomly distributed antiparallel microdomains like calcium barium niobate (CBN) [5], and strontium tetra borate (SBO) [27]. To determine the relationship of the domain structures and the polarization of the harmonics, a theoretical model has been suggested in [1]. The model mainly relies on the one-dimensional model, suggested by Le Grand *et al*. [28]. It describes the relationship between angular SHG and the domain distribution in a way called *k*-spectroscopy [29].

We consider the lateral noncollinear phase-matching condition for which the fundamental wave propagates normally to the optical axis, i.e. to the domains. The harmonics are emitted in a transverse plane over a wide emission angle. We have analyzed the polarization properties of the second- and third-harmonic by measuring the intensities with a photodiode (Coherent OP-2 VIS) behind the crystal. As an exciting beam, we use ultrashort laser pulses with a wavelength of 1500 nm, generated by a laser system consisting of a mode-locked Ti:sapphire oscillator, a regenerative amplifier, and an optical parametric amplifier. The repetition rate is 1 kHz, the pulse duration is about τ_p = 100 fs, and maximum pulse energy is about 100 µJ. Nearly transform-limited Gaussian laser pulses ($M^2 \approx 1.2$) with a diameter of about 1.5 mm are propagating without focusing perpendicular to the c-axis of the SBN crystal. The light is vertically polarized and controlled by a $\lambda/2$ waveplate. The SH and TH signals are in turn analyzed by appropriate analyzers. Transmitted light of the fundamental beam is blocked by a combination

#251216 Received 30 Sep 2015; revised 11 Nov 2015; accepted 17 Nov 2015; published 24 Dec 2015
© 2015 OSA

of appropriate color and interference filters [Fig. 2(e)]. Since the direction of the fundamental

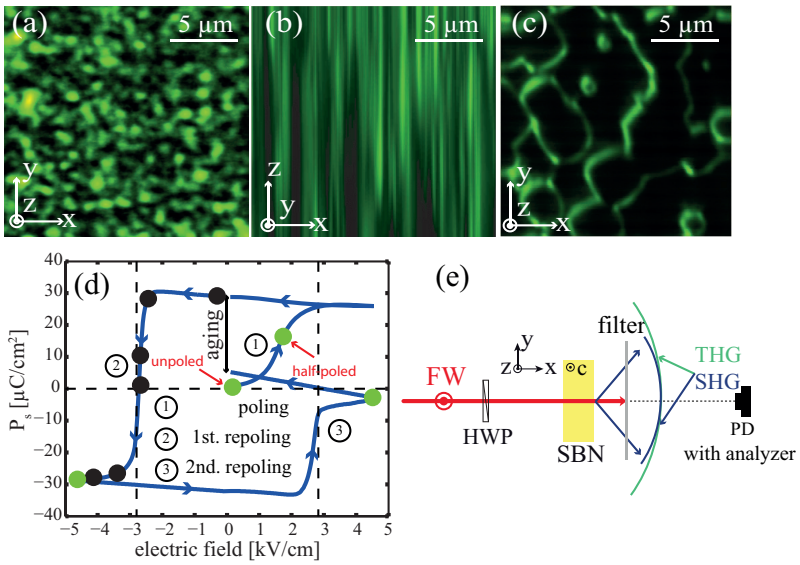

Fig. 2. (a-c) Čerenkov-type second-harmonic microscopic images of domain structures in SBN, taken using a Čerenkov SH microscope [30]. The green lines represent the domain walls. (a, b) Images of nanoscaled domains in an as-grown SBN along the optical axis and normal to the optical axis, respectively. (c) An image of microscaled domains along the optical axis in a repoled SBN. (d) Characteristic P_s-E loop of SBN: Spontansous polarization P_s in dependence of the applied electric field for three poling cycles. Green points label domain distributions at which SH signal is measured and black points label domain distributions at which TH signal is measured. (e) Schematic of the setup used to analyze the polarization; FW: fundamental wave, HWP: half-waveplate, PD: photo diode.

beam is along the crystallographic x-axis, the corresponding components of the nonlinearity tensor are d_{33} and $d_{32} = d_{24}$. An $Sr_xBa_{(1-x)}Nb_2O_6$ crystal with the dimensions 3(c)×2×4 mm, grown by the Czochralski method with a congruently melting composition $x = 0.61$ [31] has been used. The large surface parallel to the c-axis is polished to optical quality.

In preparation, the SBN sample has been initially heated above the Curie-Temperature $T_c \approx 70^\circ$ up to $\approx 200^\circ$ for 2 hours to avoid any spurious polarization and cooled down to room temperature without applying an electric field. An overview of the mechanism of creating different poling states, i.e. domain size statistics, in SBN is explained in our previous studies [6, 11]. In this paper, the polarization properties of the second-harmonic signal are handled in the first part, and of the third-harmonic signal in the second part.

3. Second-harmonic generation

As presented in [1,21], the second-harmonic intensity can be rewritten as an ensemble average of the SH emission from each domain over the domain spatial distribution in xy-plane

$$I_{(2\omega)} \propto \frac{n_{(2\omega)}}{n^2_{(\omega)}} I^2_{(\omega)} L^2 (d^{(e,o)}_{\text{eff}}(x,y) < |G(\Delta k_x, \Delta k_y)| >)^2 = \frac{n_{(2\omega)}}{n^2_{(\omega)}} I^2_{(\omega)} L^2 (\hat{d}^{(e,o)}_{\text{eff}}(x,y))^2, \qquad (1)$$

with $\hat{d}^{(e,o)}_{\text{eff}}(x,y) = d^{(e,o)}_{\text{eff}}(x,y) < |G(\Delta k_x, \Delta k_y)| >$. $G(\Delta k_x, \Delta k_y)$ represents the Fourier coefficients depending on the transverse phase mismatched. The corresponding refractive indices of the fundamental and second-harmonic waves are $n_{(\omega)}$ and $n_{(2\omega)}$, respectively. The input polarization

#251216 Received 30 Sep 2015; revised 11 Nov 2015; accepted 17 Nov 2015; published 24 Dec 2015
© 2015 OSA

angle γ is defined as the angle between the electric light field and the optical axis in z-direction. For $\gamma \neq 0$ the polarization of the SH signal consists of two components which contribute simultaneously to the strength of the generated SH signal:

$$\hat{d}^{(e)}_{\text{eff}}(x,y) = \hat{d}_{32}(x,y)\sin^2\gamma + \hat{d}_{33}(x,y)\cos^2\gamma, \tag{2}$$

and

$$\hat{d}^{(o)}_{\text{eff}}(x,y) = 2\hat{d}_{24}(x,y)\sin\gamma\cos\gamma. \tag{3}$$

In general the second-harmonic intensity is proportional to $\hat{d}^2_{\text{eff}}$ [Eq. (1)]. It can be distinguished between a coherent and an incoherent interaction between the two nonlinear polarizations. For the coherent case the total effective nonlinear coefficient has the following form

$$(\hat{d}^{(e)}_{\text{eff}}(x,y))^2 = (\hat{d}_{32}(x,y)\sin^2\gamma + \hat{d}_{33}(x,y)\cos^2\gamma)^2 = (\hat{d}_{33}(x,y))^2\left(\cos^2\gamma + \sqrt{R}\sin^2\gamma\right)^2, \tag{4}$$

In this case the two components add coherently. And for the incoherent case

$$(\hat{d}^{(e)}_{\text{eff}}(x,y))^2 = (\hat{d}_{33}(x,y))^2(\cos^4\gamma + R\sin^4\gamma), \tag{5}$$

and

$$R = \left(\frac{\hat{d}_{32}(x,y)}{\hat{d}_{33}(x,y)}\right)^2 = \left(\frac{d_{32}}{d_{33}}\right)^2\left(\frac{|G(\Delta k_x^{(oo-e)}, \Delta k_y^{(oo-e)})|}{|G(\Delta k_x^{(ee-e)}, \Delta k_y^{(ee-e)})|}\right)^2 = \frac{n^o_{(\omega)} I^{(oo-e)}_{(2\omega)}}{n^e_{(\omega)} I^{(ee-e)}_{(2\omega)}}. \tag{6}$$

Note, that the ratio of $\hat{d}_{31} = \hat{d}_{32}$ and $\hat{d}_{33}$ is not constant anymore and depends on the spatial domain distribution. It can be determined by calculating the value $(|G(\Delta k_x^{(oo-e)}, \Delta k_y^{(oo-e)})|/|G(\Delta k_x^{(ee-e)}, \Delta k_y^{(ee-e)})|)^2$ and measuring $I^{(oo-e)}_{(2\omega)}/I^{(ee-e)}_{(2\omega)}$. In the literature, this ratio is about 0.5 for SBN [32, 33] for an average domain size of 1 μm. As presented, SBN crystals provide a proper system for easily changing the domain distribution in steps. Consequently, at different poling states, different ratios of the polarization components are expected. For measuring the SH intensity of the polarization components, according to Eqs. (2) and (3), the intensity is measured only in the forward direction in order to avoid any unwanted angular effects. The corresponding mismatch vectors are $\Delta k_x^{(ee-e)} = k^{(e)}_{(2\omega)} - 2k^{(e)}_{(\omega)} = 4\pi n^{(e)}_{(2\omega)}/\lambda - 4\pi n^{(e)}_{(\omega)}/\lambda = 0.43\ \mu\text{m}^{-1}$ and $\Delta k_x^{(oo-e)} = 4\pi n^{(o)}_{(2\omega)}/\lambda - 4\pi n^{(e)}_{(\omega)}/\lambda = 0.23\ \mu\text{m}^{-1}$. Figure 3 shows measurements of the second-harmonic signals for both polarization components combined with theoretical fits corresponding to the coherent and incoherent cases [see Eqs. (4) and (5)], respectively. For the extraordinary component, the intensity indicates a characteristic variation, which can be theoretically described by the incoherent summation of the components of different processes d_{32}, d_{33} only [cf. Fig. 3(a)]. From the experimental data we obtained $R = 0.59$. It is clear that the character of those plots change significantly depending on whether the contributions from different processes add coherently or incoherently. Figure 3(b) shows the SH intensity of the ordinary process, which is fitted by Eq. (3). By poling the sample in the same manner as before, we can change this ratio R, defined in Eq. (6). This in turn will change the dependence of the SH intensity on the polarization of the fundamental wave. Figure 4 shows exemplary measurements of the extraordinary components of the output SH intensity as a function of the input polarization of the fundamental wave at four different poling states, for which the average domain sizes of about 0.25 μm, 0.8 μm, 1.5 μm, and 3.5 μm, respectively . Those poling cases are marked with green points on the hysteresis curve in Fig. 2(d). Evolution of the process “oo-e" is clearly seen in comparison to the process "ee-e". For those

#251216 Received 30 Sep 2015; revised 11 Nov 2015; accepted 17 Nov 2015; published 24 Dec 2015
© 2015 OSA

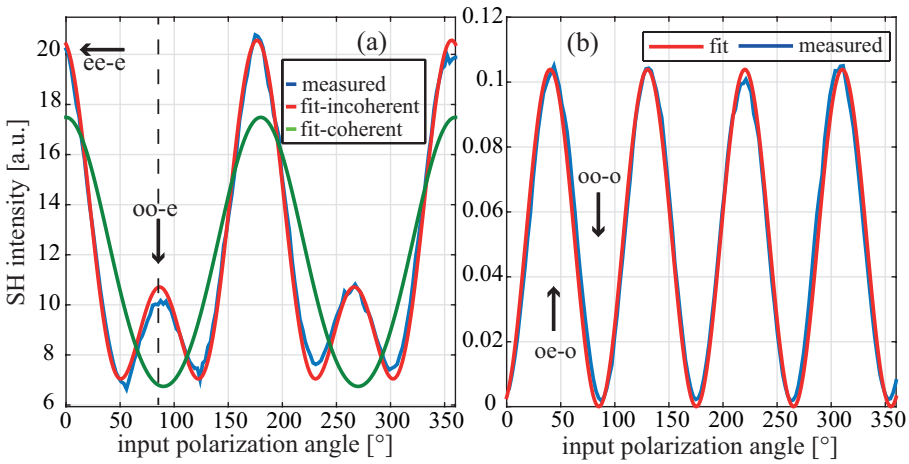

Fig. 3. Measured SH signal vs. input polarization angle γ at a fundamental wavelength 1500 nm in an SBN sample with microscaled domains. (a) for the extraordinary component; (b) for the ordinary component. In (a) the "ee-e" and "oo-e" processes are marked with arrows and in (b) the processes "oe-e" and "oo-o".

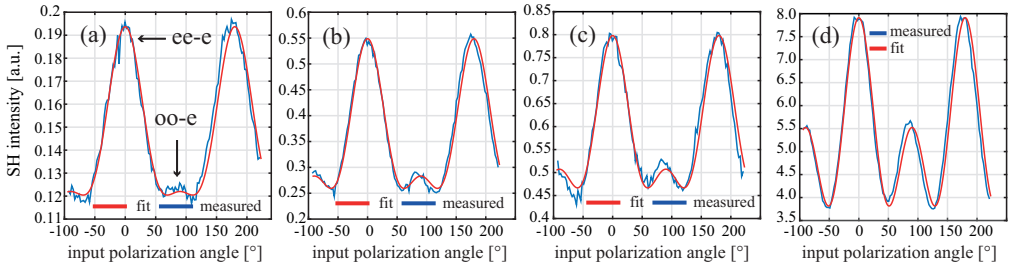

Fig. 4. Measured extraordinary SH signal vs. input polarization angle γ at a fundamental wavelength 1500 nm for (a) unpoled sample; (b) half-poled sample; (c) repoled sample; (d) two times repoled sample. Those states are marked with green points on the hysteresis curve in Fig. 2(d). The red solid curves are fits of Eq. (5) to the experimental values.

four poling states, the ratio R amounts to 0.146 for the unpoled case, 0.286 for the half-poled case, 0.35 for the repoled case, and 0.69 for the 2nd repoled case. The ordinary component of the SH process can also be measured and fitted by the intensity formulation proportional to the square of d_{24} ruled by Eq. (3). As expected, no change in relative relationship between the "oe-o" process and "oo-o" process is recorded of this polarization component when changing the domain distribution. The increasing "oo-e" component can be easily understood when looking at the corresponding Fourier coefficients (cf. Fig. 1), which are determined by $\Delta k_x^{(ee-e)}$ and $\Delta k_x^{(oo-e)}$. For microscaled domains, the Fourier coefficients, satisfying the phase-matching condition, become larger when poling and repoling the crystal [cf. Fig. 1(b)]. The entire intensity increases due to the poling dynamics during the poling process in a similar manner as in [11].

Previous measurements have shown that the polarization components can add up either incoherently [1] or coherently [25]. To verify if the pulse duration has any influence on the interaction character of the polarization components of the SHG signal, we have carried out supplementary experiments with ns-laser pulses at 1064 nm for all domain statistics reported here. In contrast to the coherent character reported in [25], our results with ns-laser pulses can

#251216 Received 30 Sep 2015; revised 11 Nov 2015; accepted 17 Nov 2015; published 24 Dec 2015
© 2015 OSA

always be described by an incoherent superposition of the nonlinear polarization for all degrees of randomness of the $\chi^{(2)}$ nonlinearity.

4. Third-harmonic generation

Due to the non-collinear nature of the harmonic generation in random nonlinear photonic crystals, the conversion efficiency of higher harmonics is quite small. However, the efficiency can be enhanced by designing the Fourier spectrum, taking into account the domain size, shape and number. As shown in the previous sections, poling and repoling the crystal changes the contribution of different nonlinear polarizations and can enhance the entire SH intensity. Under those conditions, a cascaded third-harmonic signal can also be measured. In general, third-harmonic generation can be observed in different systems, e.g. periodically poled quadratic nonlinear media. In a $\chi^{(2)}$ medium, the process is based on cascading of two quadratic effects: SHG followed by sum frequency generation (SFG) [34, 35]. In [8] was the first observation of third-harmonic (TH) signal in an as-grown sample with tightly focusing of the fundamental beam, and measured in [36]. The recorded TH signal in random nonlinear media is a result of a $\chi^{(2)}$ process, because no TH signal has been detected under the same experimental conditions using a single domain SBN crystal.

Here, the TH intensity is recorded and its polarization properties are analyzed at different poling states in order to identify the influence of the domain distribution on the TH signal properties. For this purpose, we start with an unpoled SBN sample. For this poling state, no TH signal is detected which confirms the fact that the origin of THG is not the nonlinear third-order nonlinearity $\chi^{(3)}$. The sample is then poled and repoled in order to increase the conversion efficiency of the second-harmonic generation as good as possible [11]. The switching process is continued to the point at which the SH intensity does not further increase [11]. The THG pro-

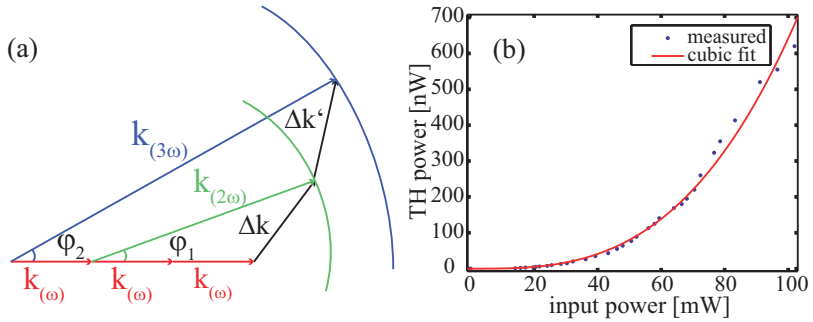

Fig. 5. (a) Diagram of the phase matching for cascaded third harmonic generation in random SBN crystal. Δk and $\Delta k'$ are phase-mismatch vectors for the second and third harmonics generation, respectively. Note the broadening of the emission angle for the THG; (b) Power of the third harmonics vs. the input power of the fundamental beam. The solid curve representing the cubic fit.

cesses involve simultaneous fulfillment of two phase matching conditions which are schematically illustrated in Fig. 5(a). As shown, the random domain distribution provides a broad set of reciprocal wave vectors which are formally determined by the Fourier spectrum of the domain structure. Those wave vectors are used to compensate for the phase mismatch Δk and $\Delta k'$. The vectors are represented by a broad circle for small domains in the Fourier space [36]. The phase-matching condition is satisfied in the area of intersection of this disk with a ring representing the spatial direction of the wave-vector of the second harmonic $k_{(2\omega)}$. As a result, the generation of the second harmonic is non-collinear with a broad spatial distribution of the

#251216 Received 30 Sep 2015; revised 11 Nov 2015; accepted 17 Nov 2015; published 24 Dec 2015
© 2015 OSA

intensity. The following second constituent process involves the interaction between the fundamental beam and the already spatially distributed second harmonic. The angular emission of the latter is now determined by the intersection of the circle with the radius $k_{(3\omega)}$ with the broad Fourier circle. The resulting spatial distribution of the generated TH is broader than that of the SH (angle $\varphi_1 < \varphi_2$). This relationship can also be changed when changing the Fourier spectrum by poling and repoling the crystal. The plot in Fig. 5(b) depicts the measured dependence of the power of the third harmonic as a function of the power of the fundamental beam. As expected, the experimental points follow faithfully the cubic fit (solid red line).

Due to the fact, that this process is of a cascaded nature, the formation of the third harmonic is a result of two quadratic processes: second harmonic generation:$E_{(2\omega)} \propto \hat{d}_{\mathrm{eff},1}(x,y)\mathbf{E}^2_{(\omega)}$ and sum frequency generation in which the third harmonic of the input field is formed by mixing of the fundamental and second harmonic waves: $E_{(3\omega)} \propto \hat{d}_{\mathrm{eff},2}(x,y)\mathbf{E}_{(\omega)}\mathbf{E}_{(2\omega)}$, where $\hat{d}_{\mathrm{eff},1}(x,y)$ and $\hat{d}_{\mathrm{eff},2}(x,y)$ are the effective nonlinearity of the constituent processes. Thus, for $\gamma \neq 0$, the polarization of the TH signal consists of two components which contribute simultaneously to the strength of the generated TH signal:

$$\hat{d}^{(o)}_{(3\omega)}(x,y) = \hat{d}_{32,1}(x,y)\hat{d}_{24,2}(x,y)\sin^3\gamma + (\hat{d}_{24,2}(x,y)\hat{d}_{33,1}(x,y) + 2\hat{d}_{24,1}(x,y)\hat{d}_{24,2}(x,y))\sin\gamma\cos^2\gamma, \tag{7}$$

and

$$\hat{d}^{(e)}_{(3\omega)}(x,y) = \hat{d}_{33,1}(x,y)\hat{d}_{33,2}(x,y)\cos^3\gamma + (2\hat{d}_{32,2}(x,y)\hat{d}_{24,1}(x,y) + \hat{d}_{32,1}(x,y)\hat{d}_{33,2}(x,y))\sin^2\gamma\cos\gamma. \tag{8}$$

Taking into account the mutually incoherent character of the contributing nonlinear processes, the TH intensity will be:

$$I^{(o)}_{(3\omega)} \propto I^3_{(\omega)}(\hat{d}^2_{32,1}(x,y)\hat{d}^2_{24,2}(x,y)\sin^6\gamma + (\hat{d}_{24,2}(x,y)\hat{d}_{33,1}(x,y) + 2\hat{d}_{24,1}(x,y)\hat{d}_{24,2}(x,y))^2\sin^2\gamma\cos^4\gamma), \tag{9}$$

for the ordinary component, and

$$I^{(e)}_{(3\omega)} \propto I^3_{(\omega)}(\hat{d}^2_{33,1}(x,y)\hat{d}^2_{33,2}(x,y)\cos^6\gamma + (2\hat{d}_{32,2}(x,y)\hat{d}_{24,1}(x,y) + \hat{d}_{32,1}(x,y)\hat{d}_{33,2}(x,y))^2\sin^4\gamma\cos^2\gamma), \tag{10}$$

for the extraordinary one. Equations (9) and (10) can be simplified into:

$$\begin{aligned} I^{(o)}_{(3\omega)} &\propto (\hat{d}^2_{32,1}(x,y)\hat{d}^2_{24,2}(x,y))I^3_{(\omega)}(\sin^6\gamma + R_1\sin^2\gamma\cos^4\gamma), \\ I^{(e)}_{(3\omega)} &\propto (\hat{d}^2_{33,1}(x,y)\hat{d}^2_{33,2}(x,y))I^3_{(\omega)}(\cos^6\gamma + R_2\sin^4\gamma\cos^2\gamma), \end{aligned} \tag{11}$$

where

$$R_1(x,y) = \left(\frac{\hat{d}_{24,2}(x,y)\hat{d}_{33,1}(x,y) + 2\hat{d}_{24,1}(x,y)\hat{d}_{24,2}(x,y)}{\hat{d}_{32,1}(x,y)\hat{d}_{24,2}(x,y)}\right)^2 = \left(\frac{\hat{d}_{33,1}(x,y) + 2\hat{d}_{24,1}(x,y)}{\hat{d}_{32,1}(x,y)}\right)^2, \tag{12}$$

and

$$R_2(x,y) = \left(\frac{2\hat{d}_{32,2}(x,y)\hat{d}_{24,1}(x,y) + \hat{d}_{32,1}(x,y)\hat{d}_{33,2}(x,y)}{\hat{d}_{33,1}(x,y)\hat{d}_{33,2}(x,y)}\right)^2, \tag{13}$$

#251216 Received 30 Sep 2015; revised 11 Nov 2015; accepted 17 Nov 2015; published 24 Dec 2015
© 2015 OSA

are complex relative strengths of the constituent nonlinear processes. For a quantitative evaluation and comparison of the entire contributions intensities, the prefactors in Eq. (11) must be also taken into account in addition to all other factors. However, as we just compare intensity ratios here we do not have to care about absolute values.

In order to get an impression of the expected evolution of the TH polarization components when changing the domain distribution, the TH intensity as a function of R_1 and R_2 is depicted in Figs. 6(a) and 6(b). In those figures, the TH signals changes in its dependence to the polarization of the fundamental beam when changing the free parameters R_1 and R_2. In general, increasing R_1 and R_2 leads to an enhancement in the process at the input polarization angle $\gamma = 45^\circ$.

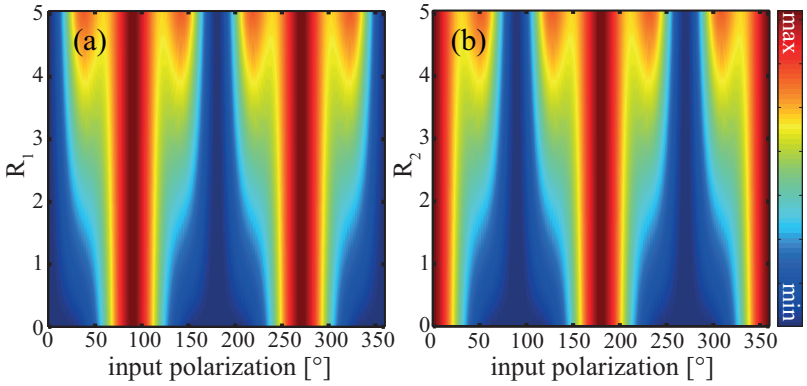

Fig. 6. Calculated TH intensity as a function of the input polarization when changing the free parameters R_1 and R_2 of the extraordinary (a) and ordinary components (b).

R_1 and R_2 are used as free parameters in fitting Eq. (11) to the experimental data in Figs. 7 and 8 for ordinary and extraordinary components, respectively. For that, the azimuthal angle γ of the linearly polarized fundamental wave is varied from zero to 360°, while the power of both, ordinary and extraordinary components of TH signals are recorded during repoling the crystal. Figures 7(a)–7(f) show exemplary the evolution of the ordinary component of the third harmonic during the repoling process at six different increasing steps of the applied field $0, 2246, 2365, 2605, 3293, 4192\,\mathrm{V/cm}$ [see Fig. 2(d)], respectively. No further changes were observed when further increasing the voltage. At 0 V [see Fig. 7], the measured third-harmonic is weak. It begins to take its form when the field is close to the coercive field. At this field, the entire TH intensity increases including all its polarization components in combination with the enhancement of the SH intensity shows in Fig. 4. The best agreement between experiment and theory is achieved for $R_1 = 1.486, 2.182, 3.240, 4.766, 4.942, 5.200$ for Figs. 7 (a)– 7(f). In all measurements the process "oe-o", consisting of the ordinary input polarization and the extraordinary second-harmonic component, is the strongest process. On the other hand, the single interaction at $\gamma = 45^\circ$ of the fundamental beam leads to an ordinary polarization component of the SH signal, which in turn interacts again with the fundamental beam, leading to ordinarily polarized TH signal. During the switching process, the TH component builds up with increasing R_1, until it becomes as strong as the “oe-o" process. This can be attributed to a faster increasing of $\hat{d}_{24,1}(x,y)$ in Eq. (12) than $\hat{d}_{33,1}(x,y)/\hat{d}_{32,1}(x,y)$, which represents the inverse root of the parameter described in Eq. (6). This remarkable behavior is not seen at the extraordinary polarization component, depicted in Fig. 8. Thus, the growth of the domain strongly influences the effective $d_{24,1}$ [see Figs. 7(d) and 7(f)], which is originally equal to $d_{32,1}$ in bulk material. Within the repoling process it is possible to see a different behavior of the

#251216 Received 30 Sep 2015; revised 11 Nov 2015; accepted 17 Nov 2015; published 24 Dec 2015
© 2015 OSA

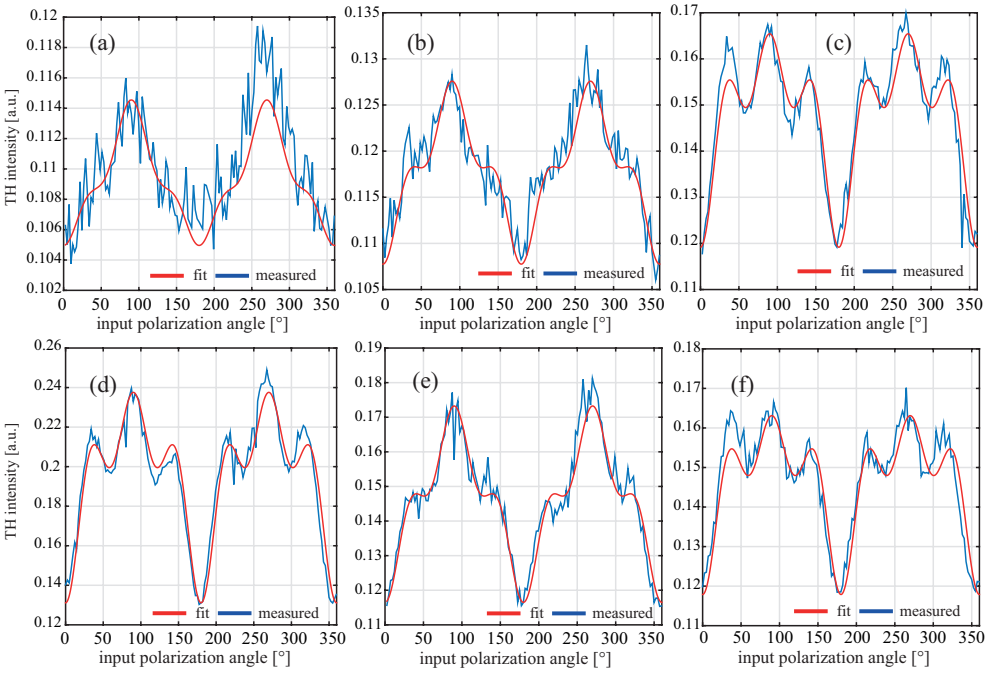

Fig. 7. The power of the ordinary component of the third-harmonic signal as a function of the input polarization angle of the fundamental beam at different poling states (a-f), in which the applied electric fields are 0 V/cm, 2246 V/cm, 2365 V/cm, 2605 V/cm, 3293 V/cm, and 4192 V/cm, respectively. An input polarization of $\gamma = 0$ corresponds to the extraordinary fundamental wave. Blue curves are experimental data; Red curves are theoretical fit according to Eq. (11).

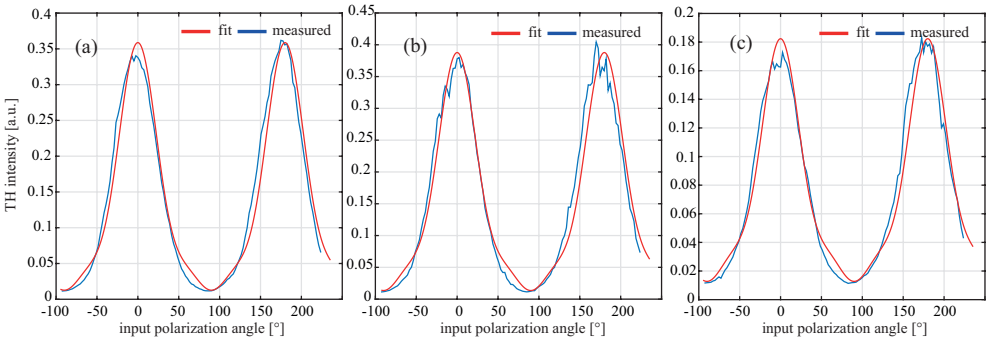

Fig. 8. The power of the extraordinary component of the third-harmonic signal as a function of the input polarization angle of the fundamental beam at different poling states (a-c), in which the applied electric fields are 0 V/cm, 2605 V/cm, and 4192 V/cm, respectively. An input polarization of $\gamma = 0$ corresponds to the extraordinary fundamental wave. Blue curves are experimental data; red curves - theoretical fits [Eq. (11)].

#251216 Received 30 Sep 2015; revised 11 Nov 2015; accepted 17 Nov 2015; published 24 Dec 2015
© 2015 OSA

intensity at $\gamma = 45^\circ$ [see Fig. 7(d)]. This can be explained by the complex switching domain dynamics for which the domain wall motion is a three-dimensional process.

For the extraordinary component, Fig. 8 shows three measurements at different poling cases. As expected, the strongest TH signals are recorded for an extraordinary fundamental wave, representing the process "ee-e".

5. Conclusion

The polarization properties of the second-harmonic signal was experimentally studied for different created domain statistics, taking into account the incoherent nature of the mutual interaction of the different polarization components of the second-harmonic signal. Changing the domain distribution redistributes the corresponding Fourier coefficients, which in turn weight the relative strength of two relevant components of the second-order susceptibility tensor. All these changes are labeled by the spontaneous polarization on the hysteresis loop. In the second part, the strengths of the third-harmonic processes can be effectively manipulated by changing the effective second-order nonlinearity. All these changes in the optical properties are restorable by tuning the spontaneous polarization, which effectively represents the disorder statistics in such random ferroelectric nonlinear crystals.

Acknowledgment

Financial support of Deutsche Forschungsgemeinschaft and Open Access Publication Fund of University of Münster is gratefully acknowledged.

#251216 Received 30 Sep 2015; revised 11 Nov 2015; accepted 17 Nov 2015; published 24 Dec 2015
© 2015 OSA